Journal of Materials Chemistry B

PAPER

View Article Online
View Journal | View Issue

Cite this: J. Mater. Chem. B, 2016, 4, 7870

Multifunctional coating based on EPC-specific peptide and phospholipid polymers for potential applications in cardiovascular implants fate†

Huiqing Chen, Yuancong Zhao,* Kaiqin Xiong, Jingan Li, Jiang Chen, Ping Yang* and Nan Huang

Received 19th July 2016,
Accepted 25th October 2016

DOI: 10.1039/c6tb01811d

www.rsc.org/MaterialsB

Surface biofunctional modification of cardiovascular implants *via* the conjugation of biomolecules to prevent thrombosis and restenosis formation and to accelerate endothelialization has attracted considerable research interest. In this study, we aimed to develop a multifunctional surface that could exhibit good hemocompatibility and function well in inducing desirable vascular cell–material interactions. The multifunctional coating (PCDLOPTPT@Ti), containing phosphorylcholine groups and endothelial progenitor cell (EPC)-specific peptides (PT), was prepared on titanium (Ti) surfaces *via* chemical conjugation. The results of platelet adhesion, activation, fibrinogen denaturation, and whole blood dynamic adhesion testing indicated that the PCDLOPTPT@Ti coating presented a better hemocompatibility when compared with bare Ti and other control samples. *In vitro* EPC and smooth muscle cell (SMC) cultures showed that the PCDLOPTPT@Ti coating significantly promoted the adhesion and proliferation of EPCs and inhibited the attachment and proliferation of SMCs. *In vivo* animal tests further confirmed that the PCDLOPTPT@Ti coating effectively inhibited thrombus formation and intimal hyperplasia while supporting endothelium regeneration. These results effectively suggest that the PCDLOPTPT@Ti coating may be promising as a coating on cardiovascular implants.

1. Introduction

Cardiovascular diseases (CVDs), mainly caused by atherosclerosis, are a leading cause of mortality.[1] Percutaneous coronary intervention using vascular stents has become the main approach for vascular stenosis in CVDs.[2] Optimal cardiovascular implant materials should perform their function without causing undue host response or inducing adverse clinical outcomes.[3,4] However, in the face of vascular endothelium injury caused by a stent implantation, the increased incidences of thrombosis, restenosis, and fibromuscular proliferation are unavoidable.[5,6] The proliferation of vascular smooth muscle cells (SMCs) is chiefly responsible for in-stent restenosis and remains a challenging clinical problem. Therefore, the application of drug-eluting stents has been reported to effectively suppress neointimal hyperplasia and accordingly reduce the in-stent restenosis rates.[7,8] However, an another issue, late-stent thrombosis, delays vascular healing and re-endothelialization.[8,9] Therefore, it is important that a favorable coronary stent should not only suppress the inflammation and SMC proliferation but also facilitate a rapid endothelialization.

As is well known, an important function of endothelial cells (ECs) is to maintain blood vessel patency and inhibit the attachment and activation of platelets by forming an endothelium monolayer as a barrier between the blood flow and the SMC underneath.[10,11] Moreover, the endothelium monolayer suppresses the attachment and proliferation of macrophages and SMCs. Thus, endowing artificial vascular stents with functions such as anti-coagulation, anti-hyperplasia, anti-inflammation, and pro-endothelialization may be a better approach for CVD therapy.[11–13]

The conjugation of biomolecules (heparin,[14] fibronectin,[3] hyaluronic acid,[15] collagen,[16] anti-CD34,[17] and REDV peptide[18]) on multifunctional surfaces is widely applied in biomedical devices and tissue engineering.[19] A significant amount of previous research has suggested the surface immobilization of specific biomolecules (antibodies,[20,21] peptides,[22,23] oligosaccharides,[24,25] and DNA-aptamers[26]) to capture endothelial progenitor cells (EPCs) from peripheral blood and induce differentiation in the autologous ECs for cardiovascular biomaterials.[27] Numerous studies have demonstrated that EPCs can differentiate into ECs *via* the induction of specific growth factors and chemokines.[28–30] Therefore, the induction of EPCs homing and adhesion may facilitate a rapid endothelialization on the surface of the

Key Lab. of Advanced Technology for Materials of Education Ministry, School of Materials Science and Engineering, Southwest Jiaotong University, Chengdu 610031, P. R. China. E-mail: zhaoyc7320@163.com, yangping8@263.net; Fax: +86-28-87600625, +86-28-87600625; Tel: +86-28-1390 8035 158, +86-28-8763 4148 802

† Electronic supplementary information (ESI) available. See DOI: 10.1039/c6tb01811d

implanted biomaterials. Depending on the selected biomolecule, the modified surface will acquire a favorable hemocompatibility[31,32] or cytocompatibility.[33,34] In our view, a promising solution is to develop a multifunctional surface that not only exhibits good hemocompatibility but also does well in modulating the vascular cell–material interactions and effectively strengthens the re-endothelialization process. In our previous study,[35] the PMMDP polymer, which was synthesized from poly(2-methacryloyloxyethyl phosphorylcholine-*co*-methacrylic acid) (PMMPC) *via* grafting dopamine (DA) and EPC-specific peptides (TPSLEQRTVYAK-GGGC-K, PT), including phosphorylcholine (PC) groups, peptides and catechol groups, was anchored onto a Ti surface to fabricate a biomimetic surface (PMMDP@Ti) that could resist platelet adhesion and enhance EPCs capture, attachment, and proliferation. The PMMDP@Ti coating exhibited good stability through mussel-inspired chemistry adhesion[36] and had the ability to inhibit SMCs adhesion and proliferation. However, the hemocompatibility, EPCs capture, adhesion, and proliferation induced by the PMMDP@Ti coating were far from reaching the clinical requirement.

It was speculated that the cellular behavior of EPCs, SMCs, platelets, and fibrinogen may be affected by the amount of exposed functional groups and biomolecules, such as PC groups and PT peptides, on the modified surface. In the present study, poly(2-methacryloyloxyethyl phosphorylcholine-*co*-methacrylic acid-*g*-dopamine) (PMMDA), PT peptides, oxidized PMMDP (POMMDP), and natural poly amino acid molecules (poly-L-lysine, PLL) were chosen as the constituents for the multifunctional coating. In particular, the surface biomolecule fixation method was changed *via* a simple layer-by-layer self-assembly based on the mussel-inspired chemistry adhesion, condensation reactions, and electrostatic interactions or hydrogen bonding interactions.[37,38] Among all the constituents, the PT peptides exhibited the highest affinity and specificity for EPCs and did not interfere with the ECs function.[8] The polymers containing 2-methacryloyloxyethyl phosphorylcholine (MPC) monomers have been applied to improve the hemocompatibility of biomaterials,[39,40] and the protein-resistant[41,42] amine-rich PLL was chosen to conjugate the biomolecules onto the materials surface.[2] Therefore, this study aims at the systematic evaluation of hemocompatibility (platelet adhesion and activation, fibrinogen denaturation and whole blood dynamic adhesion), endothelialization (EPCs adhesion and proliferation), and anti-hyperplasia (SMCs adhesion and proliferation), affected by the surface functional groups and biomolecules. In combination with *in vivo* animal tests, we have demonstrated that the multifunctional coating (PCDLOPTPT@Ti) containing phosphorylcholine groups and EPC-specific peptides effectively inhibits the thrombus formation and intimal hyperplasia and supports the endothelium regeneration.

2. Experimental section

2.1. Materials and reagents

Titanium (Ti) substrates (diameter = 10 mm) were purchased from Baoji Non-ferrous Metal Co., Ltd (Baoji Non-ferrous Metal Co., Ltd, Baoji, China). The EPC-specific peptide (PT, 99.3%) was purchased from GL Biochem Ltd (GL Biochem Ltd., Shanghai, China). Water-soluble 2-methacryloyloxyethyl phosphorylcholine (MPC, 96%) was obtained from the Joy-Nature Technology Institute (Joy-Nature Technology Institute, Nanjing, China) and used without further purification. Methacrylic acid (MA) and ethanol were purchased from Kelong Chemical Reagent Co., Ltd (Kelong Chemical Reagent Co., Ltd, Chengdu, China); MA was purified by reduced pressure distillation, and ethanol was dried over metal Na and distilled prior to use. Dopamine hydrochloride (DA, 99%), poly-L-lysine (PLL, M_W 150–300 kDa), and 1-ethyl-3-dimethylaminopropylcarbodiimide (EDC, 98%) were obtained from Sigma-Aldrich (St. Louis, USA). Modified Eagle's medium (a-MEM) and fetal bovine serum (FBS) were obtained from Hyclone (Hyclone, Utah, USA). Water-soluble tetrazolium-8 (WST-8) for the EPCs/SMCs culture and proliferation tests was obtained from BD Biosciences (San Jose, CA, USA). All other reagents were local products and of analytical grade.

2.2. Preparation of the PC/PT coating

As reported in our previous study,[35] the PMMPC polymer was synthesized by a free radical copolymerization between MPC and MA. The PMMPC grafted dopamine was named after PMMDA. The PMMDA grafted PT was named after PMMDP. POMMDP is the oxidation product of PMMDP, which is obtained by the oxidation of catechol to quinone in PMMDP.[43] A schematic of the PC/PT coating preparation is shown in Fig. 1. First, cleaned Ti sheets were immersed in a solution of PMMDA (2.0 mg mL^{-1}) at room temperature for 12 h under argon shielding to prepare the PCD@Ti sheets. Then, the cleaned PCD@Ti samples were dipped into a 0.1 mg mL^{-1} PLL solution at room temperature for 2 h to obtain the PCDL@Ti samples. Subsequently, the PCDL@Ti sheets were soaked in a 1.0 mg mL^{-1} POMMDP solution at room temperature for 2 h to prepare the PCDLOPT@Ti samples. Finally, the PCDLOPT@Ti samples were immersed in a 0.1 mg mL^{-1} PT solution at room temperature for 2 h to obtain the PCDLOPTPT@Ti samples. As each step finished, the samples were rinsed three times with deionized water to remove the unattached molecules. The immobilization of PMMDA introduces the phospholipid groups and provides the carboxyl groups for conjugation with the amino groups on the next layer of the

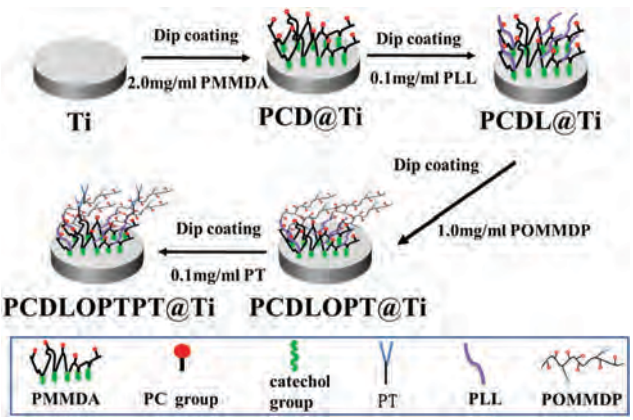

Fig. 1 A schematic for the preparation of the PC/PT coating on the Ti surface.

PLL molecules. The unreacted amino groups of the PLL conjugate with the carboxyl groups and the quinone groups of POMMDP and at the same time, introduce PT molecules and more phospholipid groups. The residual carboxyl groups of the POMMDP on the third layer can also conjugate with the amino groups of PT, and the fourth layer introduces more PT molecules.

2.3. FTIR

The changes in the surface chemical composition after PC/PT coating immobilization were determined by Fourier transform infrared spectroscopy (FTIR, Nicolet 5700 infrared spectrometer, USA) using the model of diffuse reflectance. Scanning was conducted in the range from 400 to 4500 cm^{-1}.

2.4. XPS

The surface elemental composition was confirmed by X-ray photoelectron spectroscopy (XPS, Kratos Ltd, UK) with monochromatic Mg Kα excitation radiation ($h\nu$ = 1253.6 eV). The binding energies were calibrated using the containment carbon (C1s = 284.7 eV). A Shirley background was used and the peaks were fitted using XPSPEAK 4.1 to obtain high-resolution information.

2.5. QCM-D

The amount of components coated on the titanium surface was quantified using a quartz crystal microbalance with dissipation monitoring (QCM-D, Q-Sense, Gothenburg, Sweden) at a fundamental resonant frequency of 5.0 MHz. A 5.0 MHz AT-cut quartz crystal with a gold electrode was used as the working electrode for the QCM experiments. The diameter of the quartz crystal was 13.7 mm and the diameter of the gold electrode was 5 mm. The Ti-coated (Ti/Au) QCM sensor was obtained from Q-sense (Gothenburg, Sweden).

Initially, the QCM sensor was exposed to phosphate-buffered saline (PBS, 0.067 M, pH 7.3) at a flow rate of 50.0 μL min^{-1} until a stable baseline of the QCM signal was obtained. The QCM chamber was then filled with an aqueous solution of PMMDA at 2.0 mg mL^{-1} until the frequency was relatively stable. Furthermore, the PBS solution was flowed into the chamber to replace the PMMDA solution and to wash the weakly adsorbed PMMDA from the surface. Subsequently, 0.1 mg mL^{-1} PLL solution, 1.0 mg mL^{-1} POMMDP solution, and 0.1 mg mL^{-1} PT solution were added in place of the previous solution and the previous step was repeated. The adsorbed mass (Δm) was deducted from the frequency shift (Δf) according to the Sauerbrey equation:[44]

$$\Delta m = \Delta f \times C/n \quad (1)$$

where C (C = 18.0 ng cm^{-2} Hz^{-1} at f_n = 5.0 MHz) is the mass-sensitivity constant and n (n = 1, 3, 5, ...) is the overtone number.

2.6. AFM

The surface morphology and roughness of Ti, PCD@Ti, PCDL@Ti, PCDLOPT@Ti, and PCDLOPTPT@Ti were analyzed by atomic-force microscopy (AFM, SPI 3800, NSK Inc.,) in the tapping mode. AFM was performed at room temperature in air at a rate of one line scan per second. Image analysis was performed using the CSPM Imager software.

2.7. Water contact angle

Static (sessile drop) water contact angles were measured using a goniometer with computer-assisted image analysis (JY-82, China). A droplet of ultrapure water was placed on the surface of the sample and the contact angle was determined using a horizontal microscope. For each sample, the mean value of the contact angle was calculated from at least three individual measurements taken at different locations on the examined samples.

2.8. Stability of the PC/PT coating

Every sample was immersed in 1.0 mL PBS (0.067 M, pH 7.3) using a thermostatic shaker concussion (37 °C, 60 rpm) and the soaked solution was analyzed by the UV spectroscopy every other day. After 12 days, the soaked samples were taken out and dried. The surface elemental composition of the coating before and after immersion was confirmed by XPS. In addition, the coating was washed at different flow rates of PBS and monitored using QCM-D. The functions of the coatings before and after the immersion were tested by platelet adhesion for 1 h and EPCs culture for 1 day.

2.9. Blood compatibility evaluation

Fresh human blood was obtained from the Blood Central of Chengdu, China, according to the ethical standards in place. The analysis was performed within 12 h after blood donation. Four parallel samples were used.

2.9.1. Platelet adhesion and lactate dehydrogenase (LDH) assay. Fresh human citrate-blood was added into the centrifuge tubes and centrifuged at 1500 rpm for 15 min to obtain the top layer of platelet-rich plasma (PRP). A volume of 60 μL of PRP was distributed on each surface of Ti and the samples were incubated in 24-well plates for 1 h at 37 °C. Then, the samples were carefully rinsed in 0.9% NaCl solution to remove the platelets that were not firmly adherent. After fixation with 2.5 wt% glutaraldehyde solution for 12 h, the samples were dehydrated in graded alcohol solutions (50%, 75%, 90%, and 100%; $V_{alcohol}/V_{demineralized\ water}$) and dealcoholized in the graded isoamyl acetate solutions (50%, 75%, 90%, and 100%; $V_{isoamyl\ acetate}/V_{alcohol}$). All samples were subjected to critical point drying (CPD030, BALZERS) and inspected with an optical microscope (Leica, Germany) or gold-sputtered prior to scanning electron microscopy analysis (SEM, Quanta 200, FEI, Holland) to evaluate the morphology and quantity of the adherent platelets.

An LDH assay was used to detect the amount of the adherent platelets. Briefly, 50 μL of PRP was added to the sample surfaces and incubated for 1 h at 37 °C. After rinsing with PBS, 40 μL of 1% Triton solution (Triton X-100, Sigma) was added to each sample and incubated for 5 min at 37 °C. Subsequently, 25 μL of lysate was transferred from the surfaces into a 96-well plate and 200 μL of chromogenic agent (10 mg mL^{-1} Pyr and 10 mg mL^{-1} NADH powder dissolved in Tris base buffer) was

added before testing. The absorbance of the different samples was obtained using a microplate reader at 340 nm. The amount of the adherent platelets was calculated according to the calibration curve.

2.9.2. Platelet activation and P-selectin assay. P-selectin expression was determined as a marker of platelet activation induced by the surfaces. First, 50 μL of PRP was added to the sample surfaces and incubated for 1 h at 37 °C. Then, the samples were rinsed three times with PBS and used for P-selectin immunofluorescence staining. The abovementioned samples were fixed in 4% paraformaldehyde for 12 h at room temperature and rinsed three times with PBS for 3 min each. The samples were then incubated in a goat serum (1 : 10 in PBS) for 1 h at 37 °C to block the non-specific adsorption. Subsequently, a 30 μL of mouse monoclonal anti-human P-selectin antibody (primary antibody, 1 : 200 in PBS) was added to the surfaces for 1 h at 37 °C and washed three times with PBS for 3 min each time. Thereafter, 30 μL of FITC-conjugated goat anti-mouse IgG antibody (secondary antibody, 1 : 100 in PBS) was added to the surfaces and incubated for 30 min at 37 °C and washed three times with PBS for 3 min each. Finally, the samples were observed by fluorescence microscopy (Olympus IX51, Japan).

2.9.3. Fibrinogen denaturation test. For the fibrinogen denaturation test, fresh human blood anti-coagulated with citrate was centrifuged at 3000 rpm for 15 min to obtain a platelet-poor plasma (PPP). The samples were incubated with 60 μL of PPP for 2 h at 37 °C and washed with PBS (3 × 5 min). Then, the samples were blocked with sheep serum (1 : 100 in PBS) for 30 min, three times with PBS, and incubated with 20 μL of mouse anti-human monoclonal γ-fibrinogen antibody (primary antibody, 1 : 100, product no: NYB4-2xl-f, Accurate Chemical & Scientific Corp.) for 1 h at 37 °C. Subsequently, the samples were rinsed with PBS and incubated with horseradish peroxidase-labeled goat anti-mouse antibody (1 : 100 in PBS) for 1 h. Finally, the chromogenic substrate 3,3′,5,5′-tetramethylbenzidine (TMB) was added and the reaction was stopped after 10 min using sulfuric acid. The absorbance was measured at 450 nm.

2.9.4. Whole blood dynamic adhesion test. Static and dynamic whole blood experiments were performed to comprehensively investigate the compatibility of the components of whole blood on the surface.[45] For the dynamic whole blood experiment, the samples were placed in a flow chamber and subjected to anti-coagulant fresh whole blood flow (15 dyn cm^{-2}) for 1 h. The samples were washed three times with PBS. The whole blood components on the samples were fixed with 2.5% glutaraldehyde for 2 h at room temperature. After a washing step, the platelets, erythrocytes, and plasma protein fibers attached to the samples were observed by SEM.

2.10. *In vitro* EPCs and SMCs culture

EPCs were isolated from the bone marrow of Sprague-Dawley rats (Sichuan University, Chengdu, China)[46] and cultured in single-use culture flasks with α-MEM containing 20% FBS at 37 °C in a humidified atmosphere with 5% CO_2.[47] The medium was replaced every two days. When the cells were close to confluency, they were trypsinized and cultured in α-MEM supplemented with 10% FBS and 10 ng mL^{-1} VEGF. After two weeks of culture, the cells were designated as EPCs based on the identification of their cell morphology and specific markers.

SMCs were isolated from the human umbilical artery. First, the adventitia layer and endothelium layer were stripped away from the umbilical artery. Then, the residual tissue was cut into small pieces and stuck to the bottom of a culture flask. The flask was carefully inverted and infused with a 5 mL Dulbecco's modified Eagle's medium/F12 (DMEM/F12) with 10% FBS. The flask was subsequently incubated at 37 °C in 5% CO_2 overnight and gently inverted to allow the pieces of the tissue to become fully immersed in the culture medium. The SMCs were obtained by a slow outgrowth from these tissue pieces.

All samples were sterilized by ozone before cell seeding. The EPCs and SMCs were seeded on the samples at an identical density of 5 × 10^4 cells per mL and incubated at 37 °C in 5% CO_2 for 1 and 3 days of culture. The proliferation activity of different cells on the different sample surfaces was investigated using a water-soluble tetrazolium-8 (WST-8) assay after 1 and 3 days of culture. The medium was removed and the samples were washed three times with PBS. Subsequently, fresh medium containing WST-8 reagent was added to each sample and incubated at 37 °C in 5% CO_2 for 3 h. Medium containing 10% WST-8 was used as a blank control. The absorbance was measured at 450 nm using a microplate reader. All proliferation experiments were performed in quadruplet.

Immunofluorescence staining was performed to identify the types and observe the morphology of the adherent cells on the different sample surfaces. After culturing for 1 and 3 days, the adherent cells on the samples were fixed using 2.5% glutaraldehyde at 4 °C for 6 h and rinsed with PBS. After that, the cells were stained with 50 ng mL^{-1} 4′,6-diamidino-2-phenylindole (DAPI) and 5 μg mL^{-1} 2-(6-amino-3-imino-3*H*-xanthen-9-yl)benzoic acid methyl ester (rhodamine 123) (50 μL per sample) and kept for 30 min in the dark. Fluorescent images were acquired using a fluorescence microscope (Olympus IX51, Japan).

2.11. *In vivo* animal experiments

All animal experiments were performed in accordance with the protocols approved by the Medical College of Southwest Jiaotong University, the Ethical Committee and Laboratory Administration Rules of China. *In vivo* experiments were carried out by implanting the PC/PT-modified samples into dog femoral arteries for 4 weeks. Ti was used as a positive control. Two holes with a diameter of ~0.5 mm were predrilled at either end of 3 × 5 mm^2, double-sided polished and coated samples. The Ti and modified samples were first sterilized by an ultraviolet radiation (27 W, 254 nm) for 30 min.

Two adult dogs (20–30 kg) were used in this experiment and each dog received four samples, two of each type. The samples were implanted and affixed to the inner surface of the femoral artery using a medical suture passing through the sample hole. The dogs did not receive any anticoagulation therapy after the surgery. After implantation for 4 weeks, the samples were excised and rinsed by heparin solution to remove the residual blood,

and then observed immediately using a three-dimensional microscope (Motic Image Plus 2.0 ML). Subsequently, the samples were fixed in 4% paraformaldehyde for 24 h at room temperature. After dehydration and critical point drying, the samples were observed by SEM.

2.12. Statistical analysis

The data were analyzed using the SPSS11.5 software (Chicago, Illinois, USA). Statistical evaluation of the data was performed using a Student's paired test. A probability (P) value of $P < 0.05$ was considered to be statistically significant. The results were expressed as the mean ± standard deviation (SD). All experiments were repeated three times.

3. Results and discussion

3.1. FTIR and XPS results

Changes in the surface chemical composition were analyzed by FTIR and XPS. When compared to Ti, noticeable new peaks appeared in the FTIR spectrum (Fig. 2A) of PCD@Ti, including the peaks at 1720 cm^{-1} (–COOR, –C═O), 1235 cm^{-1} (–$POCH_2$–), 1086 cm^{-1} (–$OPOCH_2$–), 1173 cm^{-1} (P═O), 969 cm^{-1} (–$N^+(CH_3)_3$), 2958, 1486, 720–790 cm^{-1} (–CH_2–), 1553 cm^{-1} (the aromatic ring), and 1639 cm^{-1} (amide I, –CONH–). These are consistent with the reported results[35] and suggest that Ti was successfully coated with PMMDA. The peaks in the range from 3420 to 3261 cm^{-1} are considered as the overlapping stretching vibrations peaks of the hydroxyl (–OH) and amine (–NH_2, –NH–) groups. The intensity of the peak at 1639 cm^{-1} (amide I, –CONH–) in the spectrum of PCDL@Ti was enhanced and a new small peak was also observed at 1520 cm^{-1} (Fig. 2B), which corresponds to the stretching vibrations of the amide II (C–N, N–H) bond. The emergence of the amine groups, amide I and amide II demonstrates the existence of PLL on the surface of PCDL@Ti.[48] The peak at 1694 cm^{-1} (Fig. 2B), which is attributed to quinone (C═O), could apparently be seen in PCDLOPT@Ti but is not obvious in the other samples.[49] This result indicates that POMMDP was introduced to the surface of PCDLOPT@Ti. According to the surface of PCDLOPTPT@Ti, the content of PT was too weak to be detected in the FTIR spectrum. XPS was required for a detailed chemical analysis of the PCDLOPTPT@Ti surface. The high resolution sulfur spectrum (Fig. 2C) shows that the peaks at 163.3 eV represent the binding energy of $S_{2P3/2}$ and the peak at 163.3 eV was attributed to the –SH group of PT on the surfaces of PCDLOPT@Ti and PCDLOPTPT@Ti.[35] The enhanced peak in the high-resolution sulfur spectra also demonstrates that more PT was introduced on the surface of PCDLOPTPT@Ti when compared to PCDLOPT@Ti. This result demonstrates that PT appeared on the PCDLOPT@Ti and PCDLOPTPT@Ti, but not on Ti, PCD@Ti and PCDL@Ti surfaces.

3.2. Quantitative analysis of the PC/PT coating

QCM-D is frequently used to investigate multilayer fabrication and the physical properties of multilayer films. In this study, the adsorptions of PMMDA, PLL, POMMDP, and PT on the substrates were monitored using QCM-D. Fig. 3 presents the curve of mass shift *vs.* time. The mass of PMMDA, PLL, POMMDP, and PT coatings sharply increased in the early stage. After the reaction, PBS was injected to remove the weakly adsorbed molecules. Finally, 247.5 ± 3.3 ng cm^{-2} PMMDA, 45.3 ± 2.8 ng cm^{-2} PLL, 73.4 ± 3.6 ng cm^{-2} POMMDP, and 28.8 ± 2.1 ng cm^{-2} PT were conjugated onto the surface of the QCM sensor coated with Ti. The result confirms the successful immobilization of PMMDA, PLL, POMMDP, and PT onto the substrate. The anchorage of PMMDA to the Ti substrate is believed to be attributed to the chemical bond between the catechol groups of PMMDA and titanium oxide, which was spontaneously formed on the surface of the Ti substrate.[50] PLL, POMMDP, and PT were fixed by the non-covalent interactions such as electrostatic interactions or hydrogen bonding.

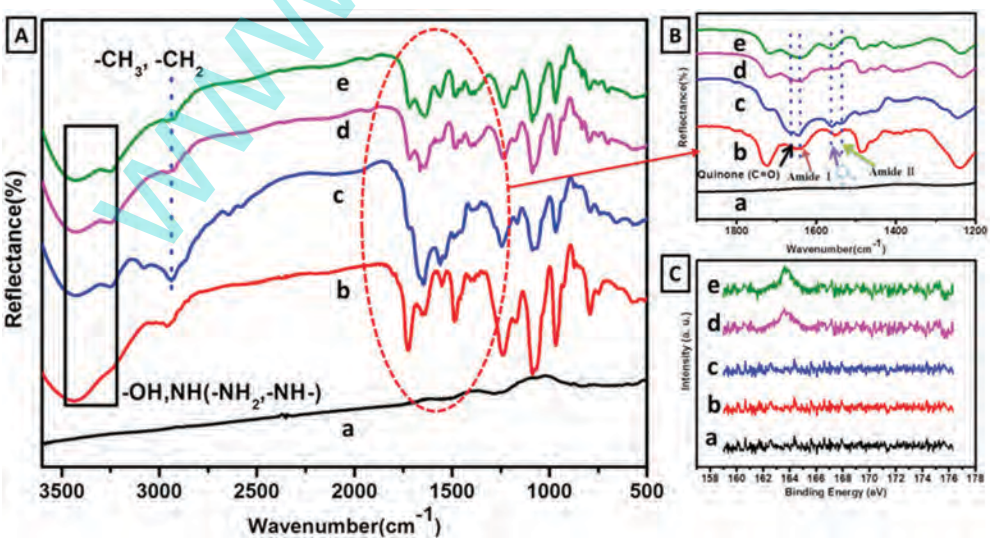

Fig. 2 (A and B) The FTIR spectra and (C) high-resolution sulfur spectrum in the XPS analysis of (a) Ti, (b) PCD@Ti, (c) PCDL@Ti, (d) PCDLOPT@Ti, and (e) PCDLOPTPT@Ti.

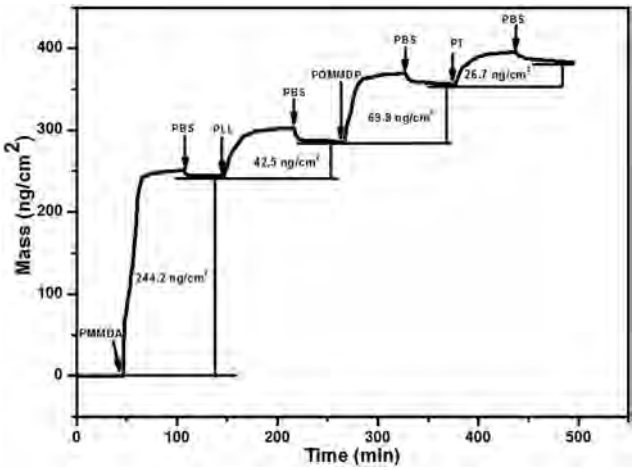

Fig. 3 The mass *vs.* time curve of PMMDA, PLL, POMMDP, and PT adsorption determined by QCM-D measurement.

3.3. Surface morphology and hydrophilicity

The morphology of the surface observed using AFM is shown in Fig. 4A. The surface of pristine Ti was smooth with an average roughness of 1.2 ± 0.2 nm, whereas the PCD@Ti (2.1 ± 0.3 nm) and PCDL@Ti (2.7 ± 0.4 nm) surfaces were rough and the PCDLOPT@Ti surface became much rougher with a relatively uniform roughness of 3.6 ± 0.5 nm. However, the roughness of the PCDLOPTPT@Ti surface was decreased to 3.0 ± 0.4 nm. These changes were attributed to the aggregation of PMMDA, PLL, POMMDP, and PT molecules, whose sizes were correlated to the amount of polymer used.[35] For implants that come in contact with blood, such as artificial heart valves and cardiovascular stents, a smooth surface is necessary with roughness values at the level of protein adsorption (<50 nm). Otherwise, platelet adhesion and thrombosis may become more obvious.[3] The slight increase in the surface roughness was well within the acceptable range.

Changes in the surface hydrophilicity may cause quantitative and qualitative variations in the absorbed proteins, which directly influence the biocompatibility of the materials.[51] The water contact angle was measured to evaluate the surface hydrophilicity before and after the biomolecule immobilization. As shown in Fig. 4B, the mean water contact angle of Ti (54.0° ± 2.4°) decreased dramatically to 40.3° ± 1.1° after coating with PMMDA (PCD@Ti). The increase in the surface hydrophilicity can be explained by the exposure of hydrophilic groups such as the PC groups of the PMMDA coating. After immobilization of POMMDP and PT, the water contact angles of PCDLOPT@Ti and PCDLOPTPT@Ti further decreased to 25.1° ± 1.3° and 28.7° ± 0.6°, respectively. This change was ascribed to the introduction of more PC groups. Hence, these findings indicate that the hydrophilicity significantly increased after the MPC polymer immobilization, and the PCDLOPT@Ti and PCDLOPTPT@Ti surfaces are more hydrophilic than the Ti surface.

3.4. Stability of the PC/PT coating

Fig. S1 (ESI†) displays the stability of the PC/PT coating assembled with PMMDA, PLL, POMMDP, and PT. It can be observed clearly that the PC/PT coating was obtained at a flow rate of 50.0 μL min^{-1} by QCM-D (Fig. S1A, ESI†). After that, the flow rate of PBS solution was adjusted to 100.0 μL min^{-1} to wash away the weakly adsorbed components from the surface for more than 2 h. However, Fig. S1A (ESI†) shows that there was no significant reduction in the PC/PT coating adsorption peaks, suggesting that the PC/PT coating exhibits a good stability. Moreover, the surface element contents of the PC/PT coatings before and after the immersion in PBS for 12 days were also examined and analyzed by XPS (Fig. S1B, ESI†). The content of nitrogen (N) in the PC/PT coating decreased from 4.75% (before immersion)

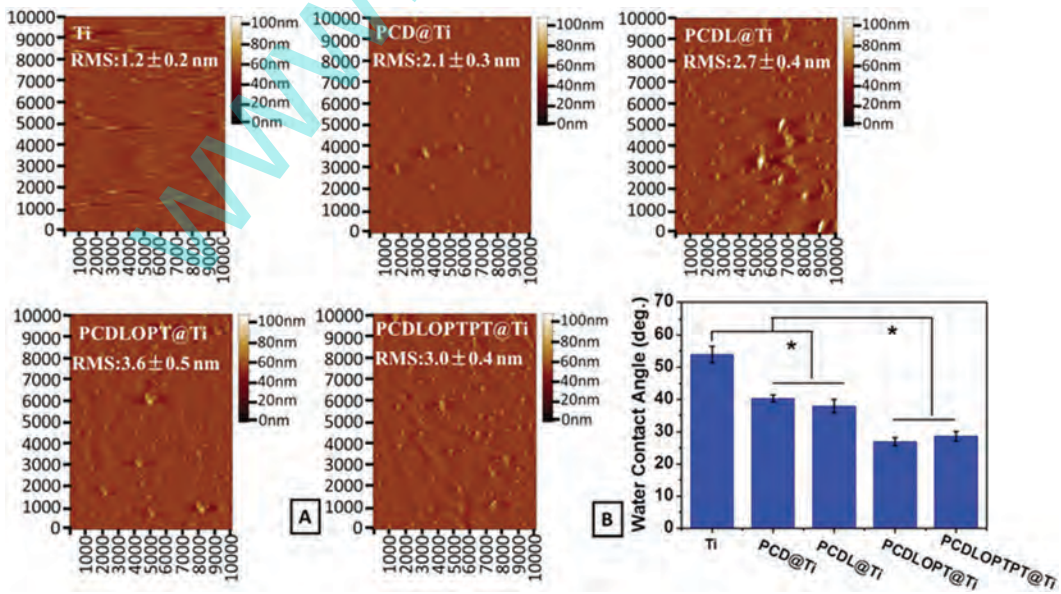

Fig. 4 The (A) AFM images and (B) water contact angle of Ti, PCD@Ti, PCDL@Ti, PCDLOPT@Ti, and PCDLOPTPT@Ti (*$p < 0.05$, mean ± SD, $N = 4$).

to 4.34% (after immersion) and the elemental sulfur content (S) from 0.65% (before immersion) to 0.59% (after immersion), showing no significant difference. In addition, the soaking solution of the PC/PT coating was investigated using ultraviolet spectroscopy (Fig. S1C, ESI†). There was no remarkable absorption peak, proving that no precipitates exist in the soaking solution. The SEM images and the amount of the adherent platelets on the sample surfaces after 1 h are shown in Fig. S1D (ESI†). There was no obvious difference in the adherent amount and activation profile on the surfaces before and after immersion. The morphology and density of the attached EPCs after 1 day of culture are presented in Fig. S1E (ESI†), showing no significant difference. All the abovementioned results indicated that the PC/PT coating on the Ti surface possessed good stability.

3.5. Blood compatibility evaluation

3.5.1. Platelet adhesion and activation. The amount and the activation profile of the adherent platelets are considered as the key indicators for the hemocompatibility evaluation of a material surface. It is generally accepted that the platelet morphology is related to its activation level. The change from a typical round shape to a dendritic shape, and then to a spread dendritic shape, spread shape, and fully spread shape corresponds to the minor to major activation stages.[52] An LDH assay was performed to semi-quantitatively evaluate the number of adherent platelets. A P-selectin assay was performed to further evaluate the platelet activation.

The SEM images of the adherent platelets on the sample surfaces after 1 h of incubation are shown in Fig. 5A. There were a large number of adherent and aggregated platelets on the Ti and PCD@Ti surfaces, and the adherent platelets mainly exhibited the spread dendritic and fully spread shapes, indicating a significant level of activation and poor hemocompatibility. However, the number of platelets on the PCDLOPT@Ti and PCDLOPTPT@Ti surfaces significantly decreased (Fig. 5A), and the adherent platelets displayed a round shape, which indicated a minor level of activation and excellent anticoagulant properties. In agreement with the SEM results, the LDH results (Fig. 5C) showed that the platelet numbers on the Ti and PCD@Ti surfaces were significantly higher ($*p < 0.05$) than that on the PCDLOPT@Ti and PCDLOPTPT@Ti surfaces. Fig. 5B shows the P-selectin immunofluorescence staining of the adherent platelets on different surfaces. When compared with Ti and PCD@Ti, the expression of P-selectin on the PCDLOPT@Ti and PCDLOPTPT@Ti surfaces was obviously decreased. The results of SEM, LDH, and P-selectin expression level further proved that the PCDLOPT@Ti and PCDLOPTPT@Ti surfaces could effectively inhibit the platelet adhesion and activation, and there was no obvious difference between PCDLOPT@Ti and PCDLOPTPT@Ti surfaces.

3.5.2. Fibrinogen denaturation. The conformational change in fibrinogen, *i.e.*, exposure of the γ chain (HHLGGAKQAGDV at γ 400–401),[53] plays a critical role in platelet activation and aggregation. Resting platelets interact with the adsorbed and denatured ones but not with the soluble fibrinogen. Fibrinogen is folded in the plasma and the small γ chain is exposed but becomes unfolded or conformationally changed when adsorbed on the foreign surfaces and the γ chain is exposed. The exposure of the protected γ chain sequences allows fibrinogen to bind to the GPIIb/IIIa integrin receptor on the platelet membrane, further causing the adhesion and aggregation of the platelets.[54] Therefore, conformational changes in fibrinogen, as measured by immunochemistry, revealed the tendency of thrombosis.

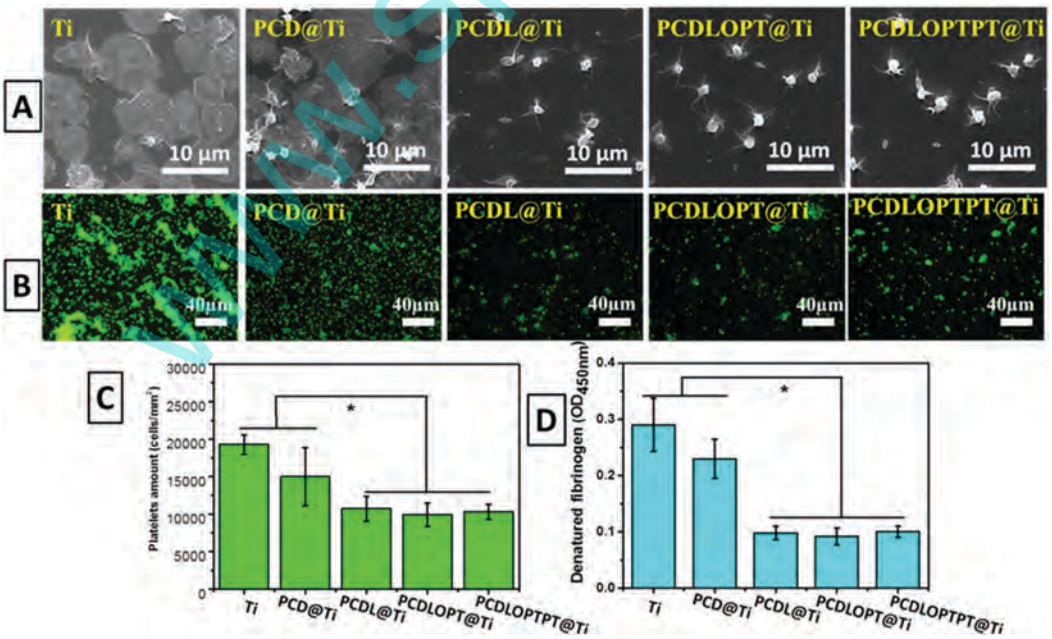

Fig. 5 (A) SEM images of the platelets on the sample surfaces after incubation with PRP for 1 h. (B) P-selectin immunofluorescence staining of the activated platelets on different sample surfaces. (C) The amount of adherent platelets on the various sample surfaces measured using the LDH assay after incubation with PRP for 1 h. (D) The denatured fibrinogen on the surface as measured by immunochemistry ($*p < 0.05$, mean ± SD, $N = 4$).

Fig. 5D displays the denaturation of fibrinogen on different surfaces. The PCDLOPT@Ti and PCDLOPTPT@Ti samples showed significantly smaller absorbance values when compared with those for Ti and PCD@Ti samples. This result demonstrates that the PCDLOPT@Ti and PCDLOPTPT@Ti surfaces decrease the denaturation of fibrinogen.

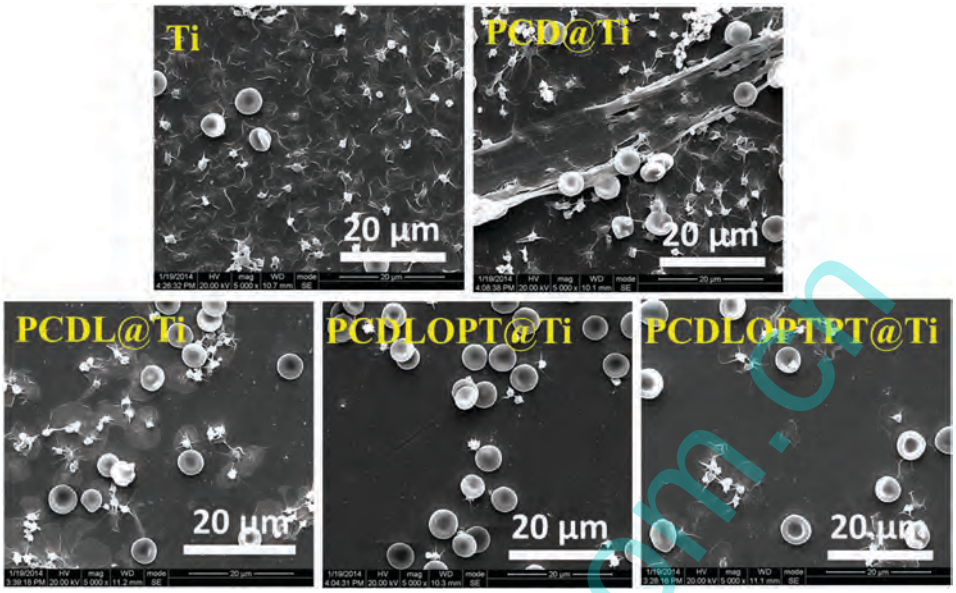

Fig. 6 The SEM images of the dynamic whole blood component adherent on Ti, PCD@Ti, PCDL@Ti, PCDLOPT@Ti, and PCDLOPTPT@Ti.

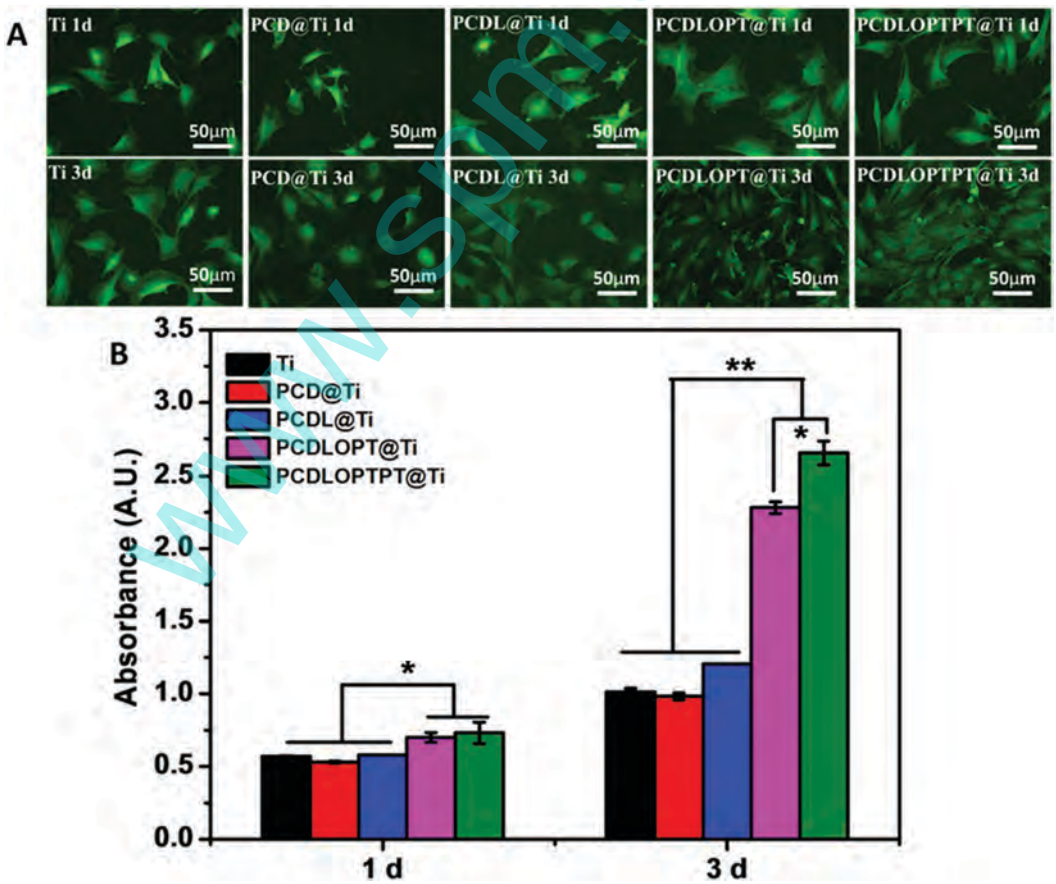

Fig. 7 (A) Rhodamine fluorescence staining and (B) proliferation of the EPCs on Ti, PCD@Ti, PCDL@Ti, PCDLOPT@Ti, and PCDLOPTPT@Ti (*$p < 0.05$, **$p < 0.01$, mean ± SD, $N = 4$).

3.5.3. Whole blood test under biomimetic blood flow. To further investigate the overall blood compatibility of the PC/PT coating, a whole blood test under biomimetic blood flow (BFSS: 15 dyn cm^{-2}) was performed, and the representative SEM images are depicted in Fig. 6. It was clear that there were more protein fibers and adherent cells (including erythrocytes and activated platelets) attached on Ti and PCD@Ti. However, the attachment of the platelets on the PCDLOPT@Ti and PCDLOPTPT@Ti surfaces was significantly reduced. Between PCDLOPT@Ti and PCDLOPTPT@Ti surfaces, there was no obvious difference. The results of the dynamic whole blood tests are consistent with those of SEM, LDH, P-selectin expression, and fibrinogen denaturation in the analysis of the static blood components. All the abovementioned results indicate that PCDLOPT@Ti and PCDLOPTPT@Ti possess a significantly better blood compatibility when compared with the other samples.

3.6. Cytocompatibility evaluation

EPCs and SMCs were seeded on the sample surfaces to evaluate the development of cytocompatibility on the PC/PT-modified surfaces. Immunofluorescence staining was used to identify the cell types and detect the morphologies of the adherent cells. A WST-8 assay was performed to investigate the cell activity.

The morphology and density of the attached EPCs are presented in Fig. 7A. The EPCs on the Ti, PCD@Ti, PCDL@Ti, PCDLOPT@Ti, and PCDLOPTPT@Ti surfaces were fusiform after 1 day of culture, followed by rapid proliferation, as observed on day 3. On the Ti, PCD@Ti, and PCDL@Ti surfaces, there were fewer adherent EPCs and some of them were round and did not spread. This difference is consistent with the result of the WST-8 assay. Fig. 7B shows the number of EPCs and their proliferation rate on the Ti, PCD@Ti, PCDL@Ti, PCDLOPT@Ti, and PCDLOPTPT@Ti surfaces. The conversion of WST-8 into the colored product was proportional to the number of cells. After 1 and 3 days of culture, the EPCs on the PCDLOPT@Ti and PCDLOPTPT@Ti surfaces exhibited distinctly enhanced attachment and proliferation when compared with those on the control Ti, PCD@Ti, and PCDL@Ti ($p < 0.05$), and there was an apparent difference between the PCDLOPT@Ti and PCDLOPTPT@Ti surfaces. The results demonstrate that the EPC-specific peptide supported the EPCs attachment and proliferation, and that there was a positive correlation between the proliferation rate and the content of EPC-specific peptides. Apparently, the biofunctional coating improves the adhesion and proliferation of EPCs.

During stent implantation, the pathological proliferation of the vascular SMCs, migrated from the injured vessel wall, results in in-stent restenosis and is the key challenge for a long-term therapy.[55,56] In this study, the growth behavior of SMCs was investigated to evaluate the anti-restenosis ability of the PC/PT coatings.

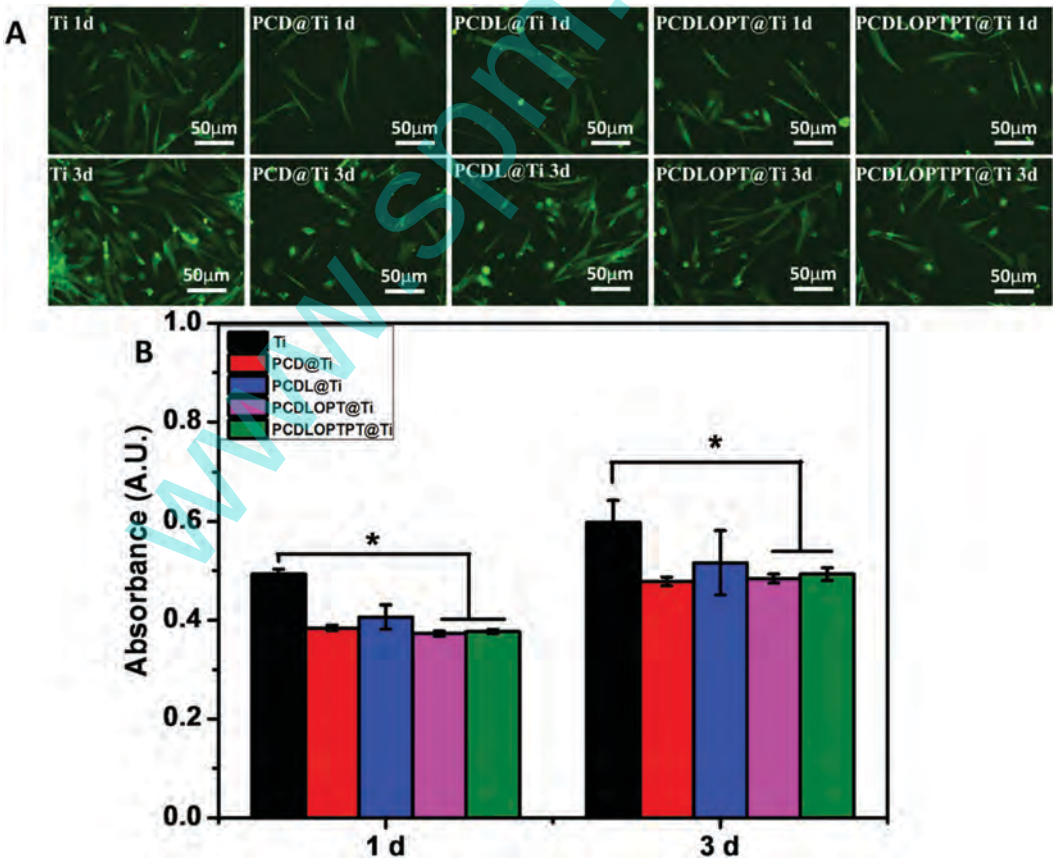

Fig. 8 (A) Rhodamine fluorescence staining and (B) proliferation of the SMCs on Ti, PCD@Ti, PCDL@Ti, PCDLOPT@Ti, and PCDLOPTPT@Ti (*$p < 0.05$, mean ± SD, $N = 4$).

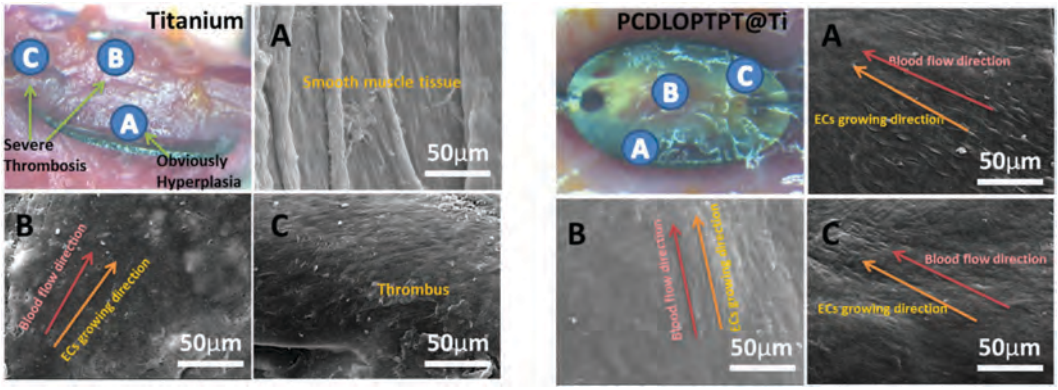

Fig. 9 The optical microscopic and SEM images of Ti and PCDLOPTPT@Ti implanted into the femoral artery of dogs for 4 weeks. Left: (A and B) The SEM image showing the morphology of the side edge tissue and the middle place tissue, respectively, and (C) the thrombus morphology at the end of the sample. Right: (A–C) The tissue morphology at the side edge, middle, and end of the samples, respectively.

The analysis of the morphology (Fig. 8A) and proliferation (Fig. 8B) of the SMCs revealed that the PC/PT coating effectively inhibited the SMCs adhesion and proliferation. This result indicates that the PC/PT coating may assist in mitigating restenosis.

3.7. *In vivo* animal tests

In vivo animal tests were performed in dog femoral arteries to further investigate the hemocompatibility and cell–material interaction on the PC/PT coatings. According to the blood compatibility and cytocompatibility evaluations, PCDLOPTPT@Ti was chosen as the sample for animal experimentation and Ti was used as the control sample. To acquire the real biological response after material implantation, the dogs did not receive any anticoagulation therapy after the surgery. Fig. 9 shows the typical optical microscopic and SEM images of the control Ti and PCDLOPTPT@Ti 4 weeks after the implantation. Evidently, there was severe thrombus formation on the Ti surface, which even extended to the inner surface of the blood vessel. In addition, a thick neointimal was formed on the Ti surface, and the tissue around the rim of the Ti disc presented a long fusiform shape in the SEM image, which resembles smooth muscle tissue and indicates serious intimal hyperplasia and incomplete endothelialization (Fig. 9). In contrast, the PCDLOPTPT@Ti surface presented no thrombus formation and the thickness of the neointimal tissue was significantly thinner than that on the Ti surface. The PCDLOPTPT@Ti surface was evenly covered by the confluent endothelium in the SEM images and a tight endothelium layer was identified, which was aligned in the direction of blood flow. The *in vivo* results demonstrate that the PCDLOPTPT@Ti surface effectively inhibits thrombus formation and intimal hyperplasia, and it supports the endothelium regeneration.

4. Conclusions

We aimed to develop a multifunctional surface that not only provides a good hemocompatibility but also functions well in inducing the desirable vascular cell–material interactions. In this study, a multifunctional PC/PT coating, containing phosphorylcholine groups and EPC-specific peptides, was prepared on the Ti surfaces *via* chemical conjugation. PCDLOPTPT@Ti not only showed a remarkable improvement in blood compatibility but also induced a considerable enhancement in the EPCs adhesion and proliferation, whereas there was a substantial inhibition of SMCs adhesion and proliferation. The *in vivo* animal test results further confirmed that the PCDLOPTPT@Ti coating effectively inhibited the thrombus formation and intimal hyperplasia while supporting the endothelium regeneration. These results effectively suggest that PCDLOPTPT@Ti may be promising when served as a coating on the cardiovascular implants.

Acknowledgements

This study was financially supported by the National Physiological Science Foundation of China (No. 30870629 and 50971107), the Key Basic Research Project (No. 2011CB606204), the Sci-technical Support Project of Sichuan Province (2013SZ0077), the Fundamental Research Funds for the Central Universities (No. SWJTU11ZT11), and the Foundation of Jiangsu Provincial Key Laboratory for Interventional Medical Devices (JR1205).

References

1 S. E. Hyman, *Sci. Transl. Med.*, 2014, **6**, 253cm9.
2 T. Liu, Y. Liu, Y. Chen, S. H. Liu, M. F. Maitz, X. Wang, K. Zhang, J. Wang, J. Y. Chen and N. Huang, *Acta Biomater.*, 2014, **10**, 1940–1954.
3 G. C. Li, P. Yang, W. Qin, M. F. Maitz, S. Zhou and N. Huang, *Biomaterials*, 2011, **32**, 4691–4703.
4 D. F. Williams, *Biomaterials*, 2008, **29**, 2941–2953.
5 A. Andukuri, M. Kushwaha, A. Tambralli, J. M. Anderson, D. R. Dean, J. L. Berry, Y. D. Sohn, Y. S. Yoon, B. C. Brott and H. W. Jun, *Acta Biomater.*, 2011, **7**, 225–233.
6 Q. Li, Z. H. Wang, S. Zhang, W. T. Zheng, Q. Zhao, J. Zhang, L. Y. Wang, S. F. Wang and D. L. Kong, *Mater. Sci. Eng., C*, 2013, **33**, 1646–1653.

7 O. Soehnlein, S. Wantha, S. Simsekyilmaz, Y. Döring, R. T. A. Megens, S. F. Mause, M. Drechsler, R. Smeets, S. Weinandy, F. Schreiber, T. Gries, S. Jockenhoevel, M. Moller, S. Vijayan, M. A. M. J. van Zandvoort, B. Agerberth, C. T. Pham, R. L. Gallo, T. M. Hackeng, E. A. Liehn, A. Zernecke, D. Klee and C. Weber, *Sci. Transl. Med.*, 2011, **3**, 103ra98.
8 Y. Yang, P. K. Qi, F. Wen, X. Y. Li, Q. Xia, M. F. Maitz, Z. L. Yang, R. Shen, Q. F. Tu and N. Huang, *ACS Appl. Mater. Interfaces*, 2014, **6**, 14608–14620.
9 A. I. Qureshi and L. R. Caplan, *Lancet*, 2013, **383**, 984–998.
10 H. Nishihara, *Adv. Drug Delivery Rev.*, 2014, **74**, 19–27.
11 F. Wu, J. A. Li, K. Zhang, Z. K. He, P. Yang, D. Zou and N. Huang, *ACS Appl. Mater. Interfaces*, 2016, **8**, 109–121.
12 R. E. Unger, K. Peters, M. Wolf, A. Mottab, C. Migliaresi and C. J. Kirkpatrick, *Biomaterials*, 2004, **25**, 5137–5146.
13 A. Lichtenberg, I. Tudorache, S. Cebotari, S. R. Lichtenberg, G. Sturz, K. Hoeffler, C. Hurscheler, G. Brandes, A. Hilfiker and A. Haverich, *Biomaterials*, 2006, **27**, 4221–4229.
14 Z. L. Yang, Q. F. Tu, J. Wang and N. Huang, *Biomaterials*, 2012, **33**, 6615–6625.
15 C. Y. Chang, A. T. Chan, P. A. Armstrong, H. C. Luo, T. Higuchi, I. A. Strehin, S. Vakrou, X. P. Lin, S. N. Brown, B. O. Rourke, T. P. Abraham, R. L. Wahl, C. J. Steenbergen, J. H. Elisseeff and M. R. Abraham, *Biomaterials*, 2012, **33**, 8026–8033.
16 Q. Z. Chen and G. A. Thouas, *Mater. Sci. Eng., R*, 2015, **87**, 1–57.
17 Q. K. Lin, X. Ding, F. Y. Qiu, X. X. Song, G. S. Fu and J. Ji, *Biomaterials*, 2010, **31**, 4017–4025.
18 Y. Wei, Y. Ji, L. L. Xiao, Q. K. Lin, J. P. Xu, K. F. Ren and J. Ji, *Biomaterials*, 2013, **34**, 2588–2599.
19 Y. Yang, P. K. Qi, Y. H. Ding, M. F. Maitz, Z. L. Yang, Q. F. Tu, K. Q. Xiong, Y. X. Leng and N. Huang, *J. Mater. Chem. B*, 2015, **3**, 72–81.
20 J. Aoki, P. W. Serruy, H. van Beusekom, A. T. Ong, E. P. McFadden, G. Sianos, W. J. van der Giessen, E. Regar, P. J. de Feyter, H. R. Davis, S. Rowland and M. J. B. Kutryk, *J. Am. Coll. Cardiol.*, 2005, **45**, 1574–1579.
21 M. W. Vaughn, L. Kuo and J. C. Liao, *Am. J. Physiol.*, 1998, **274**, H1705–H1714.
22 A. N. Veleva, D. E. Heath, S. L. Cooper and C. Patterson, *Biomaterials*, 2008, **29**, 3656–3661.
23 R. Blindt, F. Vogt, I. Astafieva, C. Fach, M. Hristov, N. Krott, B. Seitz, A. Kapurniotu, C. Kwok, M. Dewor, A. K. Bosserhoff, J. Bernhagen, P. Hanrath, R. Hoffmann and C. Weber, *J. Am. Coll. Cardiol.*, 2006, **47**, 1786.
24 L. Biancone, V. Cantaluppi, D. Duo, M. C. Deregibus, C. Torre and G. Camussi, *J. Immunol.*, 2004, **173**, 5268–5274.
25 E. J. Suuronen, P. Zhang, D. Kuraitis, X. Cao, A. Melhuish, D. McKee, F. Li, T. G. Mesana, J. P. Veinot and M. Ruel, *FASEB J.*, 2009, **23**, 1447–1458.
26 J. Hoffmann, A. Paul, M. Harwardt, J. Groll, T. Reeswinkel, D. Klee, M. Moeller, H. Fischer, T. Walker, T. Greiner, G. Ziemer and H. P. Wendel, *J. Biomed. Mater. Res., Part A*, 2008, **84**, 614–621.
27 H. E. Achneck, R. M. Jamiolkowski, A. E. Jantzen, J. M. Haseltine, W. O. Lane, J. K. Huang, L. J. Galinat, M. J. Serpe, F. H. Lin, M. Li, A. Parikh, L. Q. Ma, L. T. Chen, C. A. Milano, C. S. Wallace, T. V. Stabler, J. D. Allen, G. A. Truskey and J. H. Lawson, *Biomaterials*, 2011, **32**, 10–18.
28 X. Wang, B. Jia, Z. Chen and K. Wang, *J. Appl. Clin. Pediatr.*, 2006, **21**, 1407–1409.
29 P. Zhang, J. Wu and B. Leng, *Chin. Heart J.*, 2011, **23**, 535–537.
30 Q. Shao, C. Wang, H. Fan, M. Jiang, Y. Liu, X. Nie and L. Gao, *Chin. Heart J.*, 2006, **18**, 18–22.
31 A. Zhu, M. Zhang, J. Wu and J. Shen, *Biomaterials*, 2002, **23**, 4657–4665.
32 Z. L. Yang, J. Wang, R. F. Luo, M. F. Maitz, F. J. Jing, H. Sun and N. Huang, *Biomaterials*, 2010, **31**, 2072–2083.
33 D. Guarnieri, A. De Capua, M. Entre, A. Borzacchiello, C. Pedone, D. Marasco, M. Ruvo and P. A. Netti, *Acta Biomater.*, 2010, **6**, 2532–2539.
34 T. P. Cooper and M. V. Sefton, *Acta Biomater.*, 2011, **7**, 1072–1083.
35 H. Q. Chen, X. J. Li, Y. C. Zhao, J. A. Li, J. Chen, P. Yang, M. F. Maitz and N. Huang, *Appl. Surf. Sci.*, 2015, **347**, 169–177.
36 H. Lee, S. M. Dellatore, W. M. Miller and P. B. Messersmith, *Science*, 2007, **318**, 426–430.
37 A. I. Neto, A. C. Cibrao, C. R. Correia, R. R. Carvalho, G. M. Luz, G. G. Ferrer, G. Botelho, C. Picart, N. M. Alves and J. F. Mano, *Small*, 2014, **10**, 2459–2469.
38 J. Chen, Z. Q. Luo, Q. R. Fan, J. Y. Lv and J. J. Wang, *Small*, 2014, **10**, 4693–4699.
39 A. Lewis, L. Tolhurst and P. Stratford, *Biomaterials*, 2002, **23**, 1697–1706.
40 T. Snyder, H. Tsukui, S. Kihara, T. Akimoto, K. Litwak, M. Kameneva, K. Yamazaki and W. Wagner, *J. Biomed. Mater. Res., Part A*, 2007, **81**, 85–92.
41 W. Feng, S. Zhu, K. Ishihara and J. Brash, *Langmuir*, 2005, **21**, 5980–5987.
42 Y. C. Zhao, Q. F. Tu, J. Wang, Q. J. Huang and N. Huang, *Appl. Surf. Sci.*, 2010, **257**, 1596–1601.
43 J. Wu, L. Zhang, Y. Wang, Y. Long, H. Gao, X. Zhang, N. Zhao, Y. Cai and J. Xu, *Langmuir*, 2011, **27**, 13684–13691.
44 G. Sauerbrey, *Z. Phys.*, 1959, **155**, 206–222.
45 J. A. Li, K. Zhang, J. J. Wu, L. J. Zhang, P. Yang, Q. F. Tu and N. Huang, *Colloids Surf., B*, 2015, **128**, 201–210.
46 C. Chen, J. Y. Chen, Q. L. Li, Q. F. Tu, S. Chen, S. H. Liu and N. Huang, *Adv. Mater. Res.*, 2009, **9**, 707–710.
47 Q. L. Li, N. Huang, C. Chen, J. L. Chen, K. Q. Xiong, J. Y. Chen, T. X. You, J. Jin and X. Liang, *J. Biomed. Mater. Res., Part A*, 2010, **94**, 1283–1293.
48 T. Liu, Z. Zheng, Y. Liu, J. Wang, M. F. Maitz, Y. Wang, S. H. Liu, J. Y. Chen and N. Huang, *ACS Appl. Mater. Interfaces*, 2014, **6**, 8729–8743.
49 X. Li, L. S. H. Yuan, S. Chen, R. F. Luo., K. Q. Xiong, Z. L. Yang, J. Wang and N. Huang, *J. Mater. Chem. B*, 2015, **3**, 8717–8728.
50 Y. Yao, K. Fukazawa, N. Huang and K. Ishihara, *Colloids Surf., B*, 2011, **88**, 215–220.

51 E. Monchaux and P. Vermete, *Front. Biosci., Scholar Ed.*, 2010, 2239–2255.
52 Y. J. Weng, Q. Song, Y. Zhou, L. P. Zhang, J. Wang, J. Y. Chen, Y. X. Leng, S. Li and N. Huang, *Biomaterials*, 2011, **32**, 1253–1263.
53 M. Kloczewiak, S. Timmons, T. J. Lukas and J. Hawiger, *Biochem. J.*, 1984, **23**, 1767–1774.
54 J. N. Baumgartner and S. L. Cooper, *J. Biomed. Mater. Res.*, 1998, **40**, 660–670.
55 F. Otsuka, A. V. Finn, S. K. Yazdani, M. Nakano, F. D. Kolodgie and R. Virmani, *Nat. Rev. Cardiol.*, 2012, **9**, 439–453.
56 J. W. Jukema, T. A. N. Ahmed, J. J. W. Verschuren and P. H. A. Quax, *Nat. Rev. Cardiol.*, 2011, **9**, 79–90.